

Article

# Diamond-Bearing Root Beneath the Northern East European Platform (Arkhangelsk Region, Russia): Evidence from Cr-Pyrope Trace-Element Geochemistry

Elena V. Shchukina <sup>1,\*</sup>, Alexey M. Agashev <sup>1</sup> and Vladimir S. Shchukin <sup>2,3</sup>

<sup>1</sup> Sobolev Institute of Geology and Mineralogy, Siberian Branch of the Russian Academy of Sciences, Novosibirsk 630090, Russia; agashev.al@gmail.com

<sup>2</sup> Proex Service Ltd., Arkhangelsk 163071, Russia; vlad.shchukin@mail.ru

<sup>3</sup> AGD Diamonds, Arkhangelsk 163000, Russia

\* Correspondence: shchukinalena@igm.nsc.ru or helenashchukina@gmail.com

Received: 3 April 2019; Accepted: 26 April 2019; Published: 30 April 2019



**Abstract:** In this study, we reconstruct the composition and metasomatic evolution of the lithospheric mantle beneath the poorly-studied southern Arkhangelsk region, based on the geochemistry of 145 Cr-pyrope grains recovered from samples of modern rivers and stream sediments, to evaluate the diamond exploration potential of these territories. Based on the concentrations of Cr<sub>2</sub>O<sub>3</sub>, CaO, TiO<sub>2</sub>, and rare earth elements (REEs), the garnets are divided into four groups: (1) low-chromium lherzolitic pyropes with fractionated heavy REE patterns; (2) low- to medium-chromium pyropes of lherzolitic and megacryst associations with flat heavy REE patterns; (3) high-chromium lherzolitic pyropes with “humped” REE patterns; and (4) high-chromium and low-chromium lherzolitic and harzburgitic pyropes with sinusoidal REE patterns. The pyrope geochemistry suggests a multi-stage model for the evolution of the lithospheric mantle, including partial melting to different degrees and further metasomatic overprints by silicate and carbonatite melts. The results confirm that the lithospheric mantle beneath the study area is suitable for the formation and preservation of diamonds. The significant percentage of diamond-associated pyropes (15%) emphasizes the likelihood of high diamond contents in kimberlites to be discovered within the study area.

**Keywords:** diamond exploration; kimberlite indicator mineral; pyrope geochemistry; mantle metasomatism; lithospheric mantle; kimberlite

## 1. Introduction

The Arkhangelsk region, located in the northern portion of the East European platform, is one of the major industrial diamondiferous areas in Russia. To date, ~100 magmatic bodies (basalts, picrites, carbonatites, and melilitites, including ~70 kimberlite pipes) are known within the region. All of them are located in the north of the region forming the Arkhangelsk diamondiferous province (ADP). Two major diamond deposits exist within the ADP: the Lomonosov and Grib mines. Two kimberlite pipes (Arkhangelskaya and Karpinskogo-1) of the Lomonosov deposit (operated by Alrosa) and the V. Grib pipe (operated by Otkritie Holding) are currently being mined [1]. Since the discovery of the V. Grib kimberlite pipe in 1996, no new kimberlites have been identified within the province. However, recent results [2] show that several areas, both within the ADP and outside it, have high potentials to host local diamondiferous kimberlite sources. In this study, we present geochemical data for 145 Cr-pyrope grains recovered from heavy mineral concentrates of samples collected from modern river and stream sediments in the southern part of the Arkhangelsk region. This region is of particular

interest due to its location within the ancient Shenkursk craton, the presence of a significant number of kimberlite indicator minerals (KIMs) [2], and the lack of any known nearby magmatic bodies, including kimberlites. The geochemical composition of the Cr-pyropes is used for evaluation of the lithospheric mantle composition and assessment of its suitability for the formation and preservation of diamonds. Additionally, we discuss the origins of Cr-pyropes of different geochemical groups to reveal the types of metasomatic enrichment of the lithospheric mantle.

## 2. Geological Background and Samples

The study area (“S” area, 5673 km<sup>2</sup>) is located in the southern part of the Arkhangelsk region, hundreds of kilometers far from the ADP, within the western part of the Shenkursk craton (Figure 1).

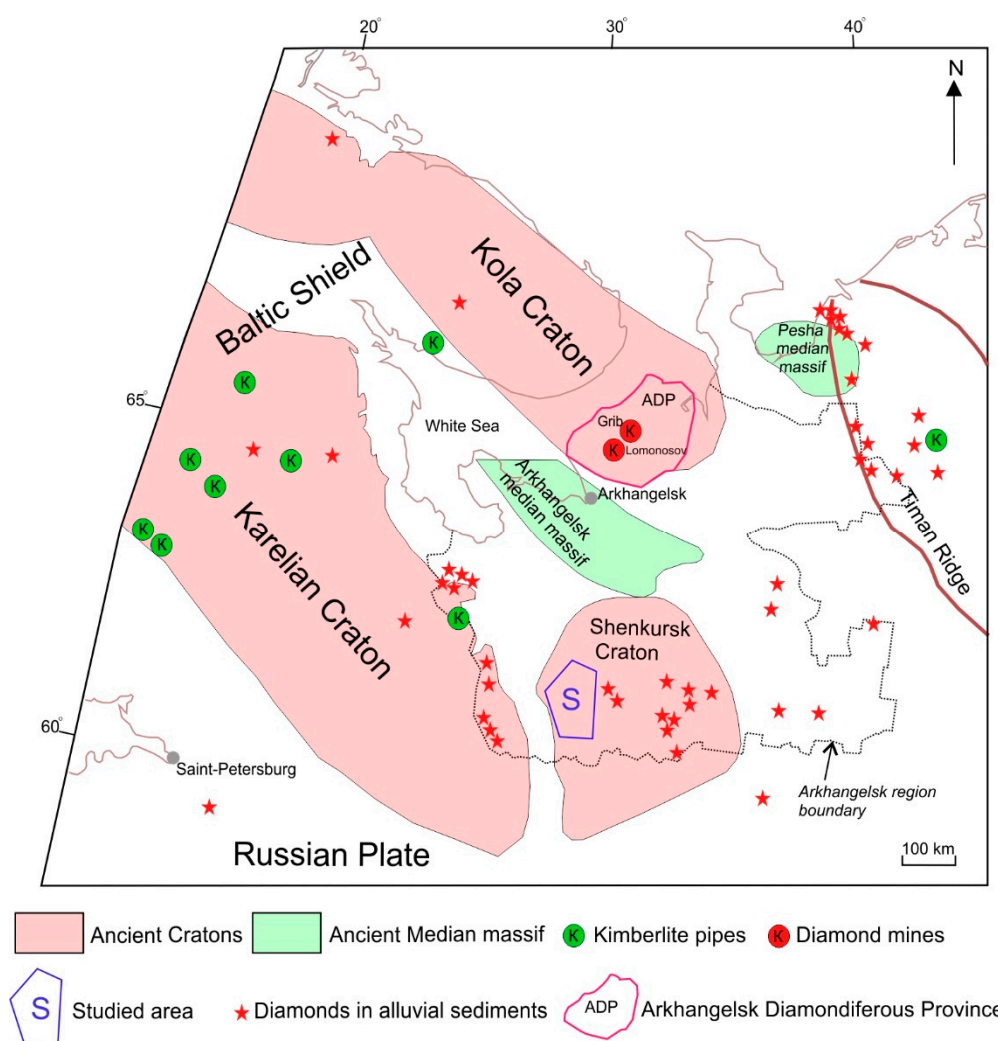


**Figure 1.** Tectonic scheme of the northern East European platform adapted with permission from [2].

The geology of this region is poorly studied, and information has not been published in open sources. Based on geophysical survey data, the upper boundary of the Precambrian basement of the “S” area occurs at a 1000–1200 m depth in the west and dips sharply towards the east to depths as great as 3000 m. The basement rocks are represented by Archaean granite-gneisses and Palaeoproterozoic metasedimentary rocks composed of metabasalts, metakomatiites, and metasandstones. The platform sediments overlie the basement rocks within the entire area and are represented by nearly horizontal layered sedimentary rocks of Vendian (mudstone, siltstone, and sandstone), Carboniferous (limestone, dolostone, and claystone), and Permian (siltstone, marl, sandstone, claystone, mudstone, dolostone,

limestone, anhydrite, gypsum, conglomerate, and breccia) periods. To date, no magmatic pipes have been discovered within this area.

It is known that the geological study of the southern Arkhangelsk region began in the late 1970s by state assignment. Afterwards, based on the results of geological and geophysical surveys and sampling surface materials (soils, stream sediments, and tills), the suggestion was first made that this area could host diamond sources [3–5]. Diamond exploration work has not been completed due to lack of funding, and the project was delayed for years. The exploration work was started again in 2005 by the “Proex Service Ltd.” geology team. During three years of field seasons, a total of 2938 samples was collected from modern river and stream sediments. A detailed description of the samples can be found elsewhere [2]. A total of 145 pyrope grains recovered from heavy mineral concentrates of alluvial samples were provided for this study. These 145 grains have morphological features that demonstrate that they are locally derived from within the studied area.

### 3. Methods

The concentrations of main elements in pyropes were analyzed at the Analytical Center for Multi-element and Isotope Research at the Institute of Geology and Mineralogy, Siberian Branch of the Russian Academy of Science (IGM SB RAS), Novosibirsk. Main element concentrations were determined at locations in polished mounted sections preselected by optical petrography. Prior to analysis, polished sections were coated with carbon to prevent charging in the e-beam. Coated sections were then introduced into a JEOL JXA-8100 electron probe micro-analyzer (EPMA, JEOL Ltd., Tokyo, Japan) operated at  $<10^{-6}$  Torr vacuum pressure, a 20-kV acceleration voltage, and a 50-nA beam current on Faraday cups, and the spot size was set to 1  $\mu\text{m}$  [6]. The instrument was equipped with five wavelength-dispersive spectrometers with various types of LIF, PET, and TAP crystals, enabling reliable analysis of elements F-U. The instrument was calibrated against in-house natural mineral standards from the IGM SB RAS reference collection. Relative standard deviations were within 1.5%. Data were acquired for 10 s on-peak as well as 10 s on either sides of the background. Raw data were corrected using a ZAF algorithm, and element abundances were transformed to oxides assuming stoichiometry, where  $\text{FeO}^{\text{T}}$  represents total iron. Detection limits were  $<0.05$  wt.% for all elements analyzed, including 0.01 wt.% for Cr and Mn, 0.02 wt.% for Ti and Na, and 0.05 wt.% for K. The main element oxide contents in wt.% were recast into atoms per formula unit (apfu) using standard protocols. More details have been reported elsewhere [6,7].

The trace element contents in pyropes were analyzed in polished sections using a Thermo Scientific XSeries 2 inductively-coupled plasma mass spectrometer (ICP-MS) equipped with the Nd:YAG LaserProbe system (Thermo Fisher Scientific Inc., Waltham, MA, USA) at the Analytical Centre of Novosibirsk State University. Prior to each spot analysis, the target area was checked in reflected and transmitted light to ensure clear, crack-free, and unaltered spots. The laser was operated at 20 Hz with a pulse energy of  $12 \text{ mJ}\cdot\text{cm}^{-2}$  and a beam size of 50  $\mu\text{m}$ . Helium was used as the gas carrier. The acquisition time was 90 s for the background and 60 s for the signal. Reference samples SRM NIST 612 and NIST 614 were used as external standards. Two analyses of the NIST 612 standard were completed before and after analysis of ten samples to correct for machine drift. The detection limits were higher for the elements of lighter mass (Sc-Sr), within 0.1–0.2 ppm, and were 0.01 ppm for elements with masses heavier than that of Sr. The low concentrations ( $\sim 0.8$  ppm) of SRM NIST 614 were analyzed three times as unknowns and gave  $<10\%$  deviation from recommended values [8] for most of the elements except Sc, Ti, Ni, and Rb, which were within 25%. The concentrations of Ca determined by EPMA were used as internal standards.

For equilibration temperatures of garnets, the Ni thermometer [9] was applied. Approximate pressure estimates were obtained from the extrapolation of pyrope  $T_{\text{Ni}}$  data to the Cr-diopside-derived geotherms of  $35\text{--}40 \text{ mW}/\text{m}^2$  [2].

#### 4. Results

The major and trace element compositions of the pyropes are presented in Table S1 in Supplementary Materials.

Following the classification scheme outlined by [10], 93% of the 145 pyropes were lherzolitic, 4% were harzburgitic, and 3% were wehrlitic (Figure 2A). Based on their C1 [11] chondrite-normalized rare earth element ( $REE_n$ ) patterns, pyropes can be classified into four principal groups (Figure 3).

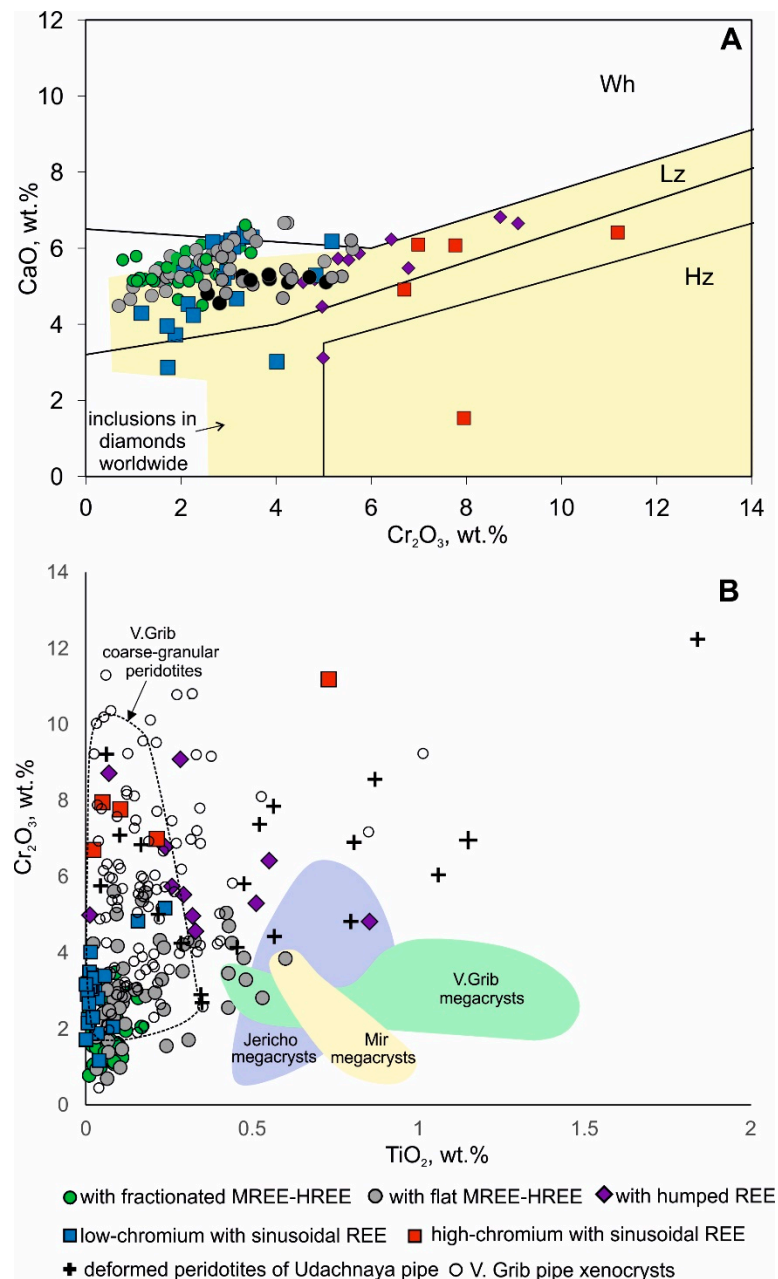


**Figure 2.** Cr<sub>2</sub>O<sub>3</sub> vs. CaO (A) and TiO<sub>2</sub> (B) of pyropes from the southern area of Arkhangelsk region compared with pyropes from: diamond inclusions worldwide [12,13], the V. Grib pipe coarse-granular peridotites [14], xenocrysts and megacrysts [15,16], Jericho [17] and Mir megacrysts [18], and Udachnaya deformed peridotites [19]. The fields for lherzolitic, harzburgitic, and wehrlitic pyropes from [10]. MREE, middle REE; HREE, heavy REE.

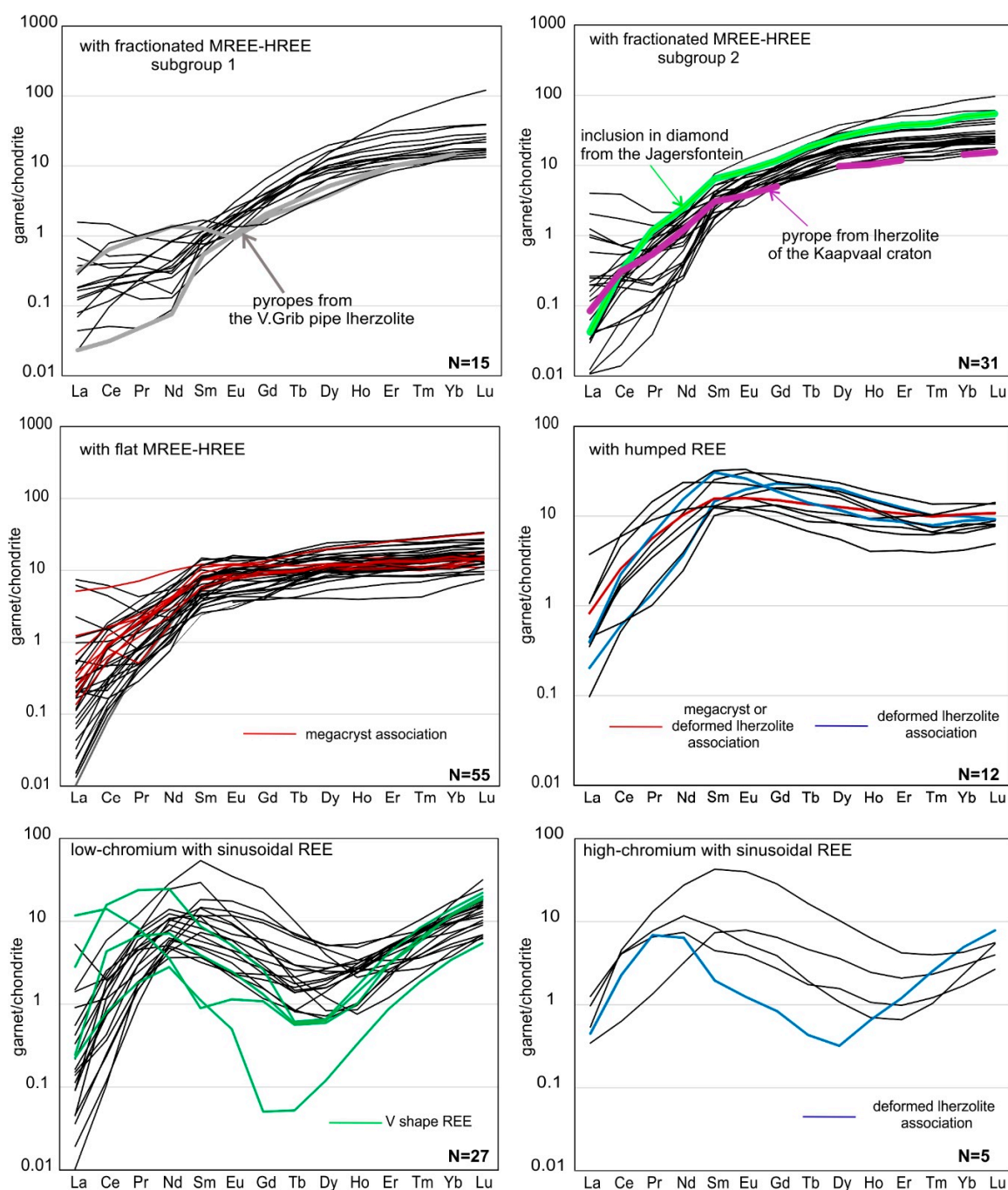


**Figure 3.** Chondrite-normalized [11] REE patterns of pyropes from the southern area of Arkhangelsk region. Pyropes from the V. Grib pipe lherzolites [14], inclusion in diamond from the Jagersfontein [20], and pyrope of lherzolite from the Kaapvaal craton [21]. N, number of grains analyzed.

#### 4.1. Pyropes with Fractionated MREE-HREE Patterns

The first group (32% of the total population, here and afterwards) was represented by pyropes that have fractionated patterns from middle (M) REEs to heavy (H) REEs ( $Yb_n = 15\text{--}100\times$  chondritic). Based on their MREE contents, this group can be subdivided into two subgroups. The first subgroup contained grains with low MREE concentrations ( $Sm = 0.04\text{--}0.2$  ppm) near C1 chondrite values and  $Yb_n/Sm_n$  ratios of 10–121 (average  $Yb_n/Sm_n = 33$ ). These pyropes were low in Zr (0.3–7 ppm); the Y content varied within the range of 7–46 ppm (Figure 4). The second subgroup was composed of pyropes with elevated MREE contents ( $Sm_n = 2\text{--}9\times$  chondritic) and  $Yb_n/Sm_n$  ratios of 4–16 (average

$Yb_n/Sm_n = 9$ ). Compared to the pyropes with low MREEs, the pyropes of the second subgroup were also different in having higher Zr (8–33 ppm). The style of light (L) REE patterns (Figure 3) varied from positive ( $La_n/Nd_n = 0.01–0.5$ ) to nearly flat ( $La_n/Nd_n \sim 1$ ) to negative slopes ( $La_n/Nd_n > 1$ ) in the two subgroups.

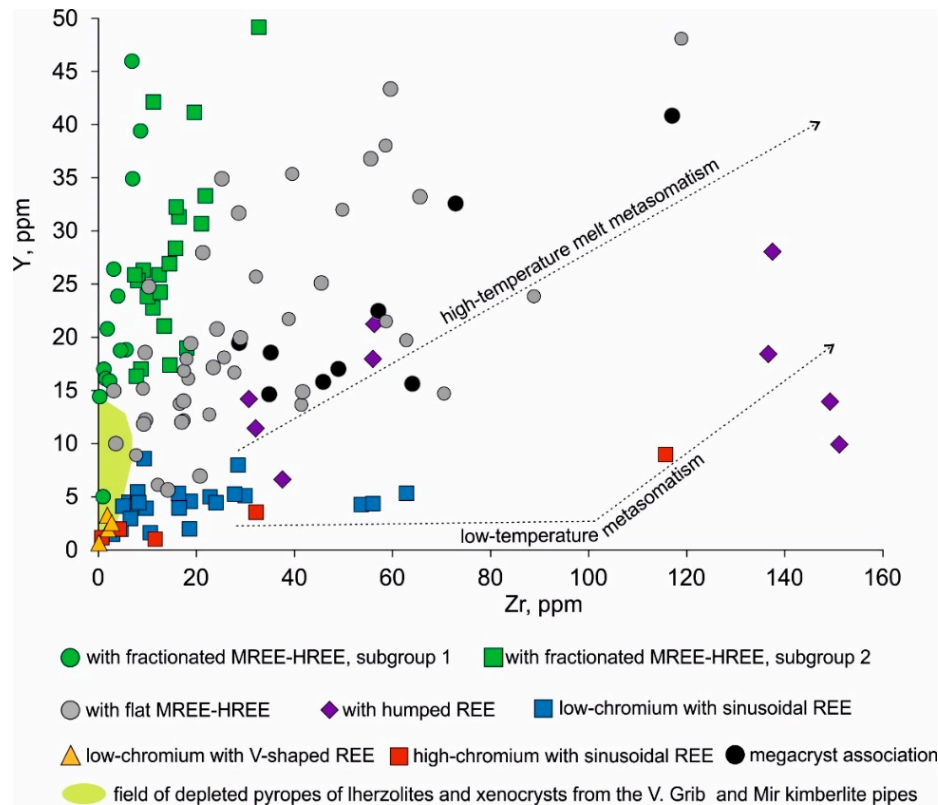


**Figure 4.** Y vs. Zr in pyropes from the southern Arkhangelsk region. Pyropes from the V. Grib pipe lherzolites and xenocrysts [14,15] and xenocrysts of the Mir pipe [18]. Trends of high- and low-temperature metasomatism [21].

On the  $Cr_2O_3$  vs. CaO diagram, pyropes of the first group matched the low-chromium ( $Cr_2O_3 = 1–3.5$  wt.%; average  $Cr_2O_3 = 2.1$  wt.%) lherzolitic field (Figure 2A). Additionally, these pyropes had low  $TiO_2$  content ( $TiO_2 < 0.1$  wt.%; Figure 2B). The magnesium number ( $Mg\# = (Mg/(Mg + Fe)) \times 100$ ) was within the range of 78–84. Two grains (Nos. 177 and 206) from the first subgroup were very low in  $Cr_2O_3$  content ( $Cr_2O_3 = 0.7–1.0$  wt.%) and  $Mg\#$  ( $Mg\# = 76$  and  $69$ , respectively), which is a feature of websteritic garnets [12,13]. Compared to websteritic garnet inclusions in diamonds, these two grains did not contain  $TiO_2$  ( $TiO_2 = 0.01–0.02$  wt.%). The pyropes of the first group showed a small range of Ni content (15–38 ppm), which corresponded to estimated temperatures of 800–1000 °C (Figure 5).

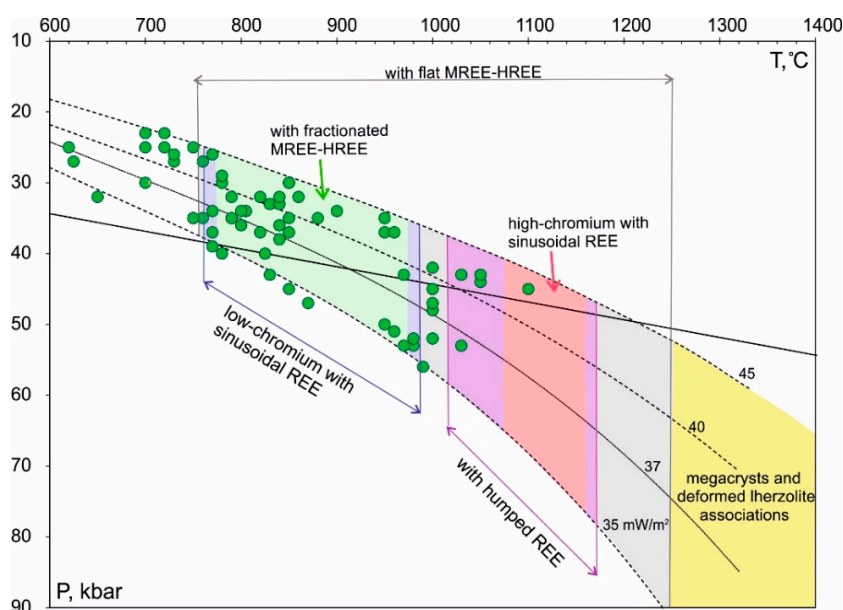


**Figure 5.** The extrapolation of pyrope  $T_{Ni}$  [9] data to the Cr-diopside-derived (green circles) geotherms [2]. Geotherms from [22].

#### 4.2. Pyropes with Flat MREE-HREE Patterns

The pyropes of the second group (38%) had flat  $REE_n$  patterns from MREE to HREE (Figure 3) with  $Yb_n/Sm_n < 5$  (average  $Yb_n/Sm_n = 2.3$ ). The concentrations of HREEs were within the range of 5–40 $\times$  chondritic. Compared to pyropes with fractionated MREE-HREE patterns, these grains were different in having higher Y (5–48 ppm) and Zr (3–118 ppm) contents and positive Y/Zr correlations (Figure 4). Most of these grains were depleted in LREEs ( $La_n = 0.01$ – $1.2\times$  chondritic) and had a positive slope from LREEs to MREEs.

On the  $Cr_2O_3$  vs. CaO diagram, pyropes of the second group matched the field of low- to medium-chromium lherzolitic pyropes ( $Cr_2O_3 = 0.6$ – $5.9$  wt.%;  $CaO = 4.4$ – $6.2$  wt.%). Two grains were slightly enriched in CaO (6.7 wt.%) and matched the “wehrlite” field. Half of the pyropes of the second group overlapped those with fractionated MREE-HREE patterns, forming a strong positive trend towards the “wehrlite” field. The other half had higher  $Cr_2O_3$  contents accompanied by slightly increasing CaO concentrations, forming a gentler positive trend towards the high-chromium lherzolitic field. The Mg# was within the range of 79–86. Most pyropes had low to moderate  $TiO_2$  contents (0.01–0.3 wt.%), which positively correlated with Mg#. Nine grains were enriched in  $TiO_2$  (0.4–0.6 wt.%), had negative  $TiO_2/Mg\#$  correlations, and can be related to megacryst association. The Ni contents varied within a wide range (15–227 ppm) and positively correlated with  $TiO_2$  contents. Pyropes with  $TiO_2 < 0.1$  wt.% had Ni contents of 15–48 ppm, which corresponds to estimated temperatures of 770–1085 °C. Pyropes that were enriched in  $TiO_2$  ( $TiO_2 > 0.3$  wt.%) had the highest Ni contents (Ni = 74–227 ppm), corresponding to a temperature  $T > 1300$  °C. Pyropes with  $0.1 < TiO_2 < 0.3$  wt.% had Ni contents of 18–76 ppm, corresponding to temperatures of 800–1250 °C.

#### 4.3. Pyropes with Humped REE Patterns

The pyropes of the third group (8%) had positive slopes from LREEs to MREEs ( $Sm_n/La_n = 3$ – $76$ ) with peaks in Sm–Eu–Gd, followed by negative slopes from MREEs to HREEs with a trough in Ho ( $Ho_n = 4$ – $19\times$  chondritic), and a nearly flat slope from Ho to Lu ( $Lu_n/Ho_n = 0.6$ – $1.5$ ; Figure 3). These pyropes had elevated Zr contents (Zr = 30–236 ppm); the Y contents varied in the range of 6–28 ppm (Figure 4).

All the grains of this group contained moderate to elevated concentrations of  $Cr_2O_3$  (4.6–9.1 wt.%), and on the CaO vs.  $Cr_2O_3$  diagram, they matched the lherzolitic field with the exception of one grain,

which plotted in the harzburgitic field (Figure 2A). The TiO<sub>2</sub> contents were mostly low to moderate (TiO<sub>2</sub> = 0.01–0.3 wt.%; Figure 2B). One of the pyropes (No. 203) was enriched in TiO<sub>2</sub> (TiO<sub>2</sub> = 0.85 wt.%) with moderate Cr<sub>2</sub>O<sub>3</sub> content (Cr<sub>2</sub>O<sub>3</sub> = 4.8 wt.%) and can be related to megacryst or deformed lherzolite associations. Two other grains (Nos. 44 and 174) had elevated concentrations of Cr<sub>2</sub>O<sub>3</sub> (Cr<sub>2</sub>O<sub>3</sub> = 6.4 and 5.3 wt.%) and TiO<sub>2</sub> (TiO<sub>2</sub> = 0.6 and 0.5 wt.%) and can be related to deformed lherzolites (Figure 2B). The Mg# varied within the range of 81–86 for all grains. The Ni contents varied within the range of 40–107 ppm, which gave a temperature range of 1000–>1300 °C (Figure 5).

#### 4.4. Pyropes with Sinusoidal REE Patterns

Pyropes of the fourth group (22%) had sinusoidal REE patterns and can be subdivided into two subgroups. The first subgroup was represented by grains that had strongly-positive slopes from LREEs to MREEs (average Sm<sub>n</sub>/La<sub>n</sub> = 90), followed by strong negative slopes from MREEs to HREEs with a trough in Dy or Ho at 0.6–5× chondritic, and then pronounced positive slopes in HREEs (Lu<sub>n</sub>/Ho<sub>n</sub> = 4–40; Figure 3). Four grains (Nos. 45, 81, 96, and 150) were enriched in LREEs (La<sub>n</sub> = 0.2–12× chondritic) and had V-shaped REE patterns with Gd-Tb-Dy values of 0.05–2× chondritic. Pyropes with V-shaped REE patterns contained the lowest Zr (0.1–2 ppm) and Y (0.6–3 ppm) concentrations. Other pyropes were low in Y (1.6–8.5 ppm); the Zr contents varied within the range of 3–63 ppm (Figure 4). On the Cr<sub>2</sub>O<sub>3</sub> vs. CaO diagram, pyropes of the first subgroup matched the low-chromium lherzolitic and harzburgitic fields (Cr<sub>2</sub>O<sub>3</sub> = 1.2–5.2 wt.%, CaO = 2.8–6.2 wt.%). These pyropes had low TiO<sub>2</sub> contents (<0.08 wt.%). One grain (No. 147) matched the “wehrlitic” field and had a higher TiO<sub>2</sub> content (TiO<sub>2</sub> = 0.2 wt.%). The Mg# varied within the range of 81–84, with the exception of one grain (No. 5), whose Mg# was much lower (Mg# = 73). The Ni contents varied within a small range of values from 13–30 ppm, corresponding to calculated temperatures of 750–980 °C (Figure 5). The “wehrlitic” pyrope had elevated Ni content (134 ppm), giving an estimated temperature >1500 °C.

The pyropes of the second subgroup had smoother sinusoidal REE patterns. These samples had positive slopes in LREEs (La<sub>n</sub>~chondritic values) with a peak in Nd or Sm at 7–43-times chondritic abundance, followed by negative slopes from MREEs to HREEs with a trough in Er<sub>n</sub> (Er<sub>n</sub> = 0.7–4.2× chondritic). The styles of HREEs varied from nearly flat (Lu<sub>n</sub>/Er<sub>n</sub> = 1.3 and 1.9) to markedly positive (Lu<sub>n</sub>/Er<sub>n</sub> = 2.7 and 8.2). One of the grains (No. 121) had a V-shaped REE pattern with peaks in Pr (Pr<sub>n</sub> = 7× chondritic) and Lu (Lu<sub>n</sub> = 8× chondritic) and a trough in Dy (Dy<sub>n</sub> = 0.3× chondritic). The pyropes of the second subgroup were low in Y (Y = 1–9 ppm), but had variable Zr contents (Zr = 0.7–116 ppm). On the Cr<sub>2</sub>O<sub>3</sub> vs. CaO diagram, the grains matched the high-chromium lherzolitic and harzburgitic fields (Cr<sub>2</sub>O<sub>3</sub> = 6.7–11.2 wt.%, CaO = 1.5–6.4 wt.%). The TiO<sub>2</sub> contents varied within the range of 0.02–0.2 wt.%. One of the grains (No. 121) had simultaneous enrichment in TiO<sub>2</sub> (0.7 wt.%) and Cr<sub>2</sub>O<sub>3</sub> (11.2 wt.%) contents, and this feature was documented only for garnet from deformed peridotite samples from the base of the lithospheric mantle [19]. The Mg# varied within the range of 80–88. All of the grains had elevated Ni contents of 48–60 ppm with a maximum value of 127 ppm in the pyrope of the “deformed lherzolite” association, corresponding to temperature parameters of 1070–1160 °C and >1500 °C, respectively.

## 5. Discussion

### 5.1. Origin of Pyropes

We discuss the origin of each geochemical type of pyrope with the aims of reconstructing the melting and metasomatic history of the host rocks and evaluating the metasomatic processes in the lithospheric mantle beneath the study area.

Pyropes in cratonic lithospheric mantle may have different origins: (1) residues after melt extraction [15,23], (2) grains exsolved from high-temperature orthopyroxene upon cooling [24], (3) products of the reaction orthopyroxene + spinel = garnet + olivine [25], and (4) metasomatic minerals formed under the influence of silicate and carbonatite melts [19].

Low-chromium pyropes with fractionated MREE-HREE patterns make up a large part (32%) of the studied grains. However, this type of pyrope is not widespread among mantle peridotites, xenocrysts, and diamond inclusions worldwide. We have found a few examples reported in the literature: (1) pyropes of six lherzolites and one pyrope xenocryst from the V. Grib pipe [14,15] and one Cr-poor lherzolitic pyrope inclusion in diamond from the Victor mine (VMG327-1 pyrope [26]), which were equivalent to the MREE-depleted subgroup (Figure 3); and (2) websteritic garnet inclusions in diamonds from Jagersfontein (JF 122 pyrope [20]) and one pyrope from lherzolites of the Kaapvaal craton (PR90-57 [27]), which were equivalent to the MREE-enriched subgroup. However, our recent study revealed a high proportion of this type of garnet in the Mir pipe (Siberian craton) kimberlites [18]. The preservation of fractionation in HREE patterns of these pyropes can be regarded as a sign of an ancient melt extraction event that affected the primitive mantle source [12]; i.e., these pyropes could be of residual nature. Most grains with low MREEs (Subgroup 1) contained low Zr (<8 ppm) and Y (<20 ppm) contents and matched the field of “depleted” pyropes from the V. Grib lherzolites [14]. The increase in Y contents (20–48 ppm) in other grains of this subgroup accompanied a La increase. Additionally, LREE enrichment was observed in the REE patterns of most of the pyropes of this subgroup, similar to those in several “depleted” pyropes of the V. Grib lherzolites. Therefore, pyropes with strong positive slopes from LREEs to HREEs and with low Y and Zr contents can be regarded as residues with no significant influence of metasomatic enrichment. The increase in the degree of metasomatic enrichment was marked by increases in Y and LREEs. Pyropes with elevated MREEs (Subgroup 2) also had higher Zr (8–36 ppm) and Y (17–70 ppm) contents, which positively correlated with Sm, and on the Y-Zr diagram, they formed a trend parallel to pyropes of the first subgroup and apparently marked an increase in the degree of metasomatic enrichment by LREE-enriched melt/fluid. Most grains from the first subgroup contained  $\text{TiO}_2 < 0.04$  wt.%, which can rule out metasomatic enrichment [28]. In contrast to these grains, most of the pyropes from the second subgroup contained  $\text{TiO}_2 > 0.04$  wt.%, confirming some metasomatic enrichment. All “depleted” pyropes were low in  $\text{Cr}_2\text{O}_3$  contents, which indicates low degrees of partial melting.

Low-chromium pyropes with flat MREE-HREE patterns were the largest population of pyropes (38%) from the study area. Such pyropes are most common within fertile (or refertilized) lherzolite xenoliths from kimberlite localities worldwide; they are in major and trace element equilibrium with coexisting clinopyroxene [29]. These pyropes showed progressive increases in Y and Zr corresponding to high-temperature metasomatic trends [21], and the metasomatic agent could have silicate composition, most likely basaltic composition [15,19,29]. This type of metasomatic enrichment produced the most significant changes in modal mineralogy and geochemistry of peridotites because the reaction of such a silicate melt with initially depleted peridotite produces enrichment of the rocks in clinopyroxene and garnet and consequently in middle and heavy REEs, Y and Zr [19]. The high- $\text{TiO}_2$  pyropes of megacryst association also formed during the high-temperature metasomatism and were directly crystallized products of silicate melts. The composition of these melts is a matter of debate between two major points of view. The first interpretation [17,30] suggests crystallization of megacrysts directly from kimberlite magma. The other viewpoint assumes that these megacrysts crystallized from an asthenospheric melt with a composition close to that of ocean island basalt [19,31,32] or picrite [15,18]. The Nd isotope compositions of kimberlites and megacrysts were close; therefore, the original magma for megacrysts and kimberlites had the same asthenospheric source [33].

High-chromium pyropes with humped REE patterns have also been reported in lherzolite xenoliths worldwide [13–15,23]. No clinopyroxene showed trace element equilibria with such garnet in peridotites [33]. In the V. Grib pipe lherzolites, these garnets were associated with clinopyroxenes that contained moderate LREEs (10–40× chondritic) and were in trace element equilibrium with silicate melt of basaltic composition. In these lherzolites, garnet was in trace element disequilibrium with coexisting clinopyroxene [14]. The pyropes with humped REE patterns did not show significant depletions in LREEs, indicating that clinopyroxene formation was rare at this stage of metasomatism. The enrichments in HREEs in the pyropes indicated the silicate composition of the metasomatic

agent, which nevertheless must be enriched in LREEs. For the V. Grib peridotites, the composition of the parental melt for pyropes with “humped” REE patterns was concluded to be close to that of picrite [15], whereas for the Udachnaya peridotites, the parental melt composition was close to that of kimberlite [29].

High-chromium pyropes of harzburgitic and lherzolitic parageneses with sinusoidal REE patterns have been well documented among all kimberlite provinces worldwide and are the main types of garnet inclusions in diamonds [12,13,28]. These pyropes are now generally accepted to have initially formed in a highly-depleted (>35–50%) mantle source (clinopyroxene-free harzburgites) under the influence of C–H–O melts/fluids with high LREE/HREE ratios [12,13,28], most likely due to carbonatite composition [34]. According to recent experimental results [35], the crystallization of high-chromium harzburgitic pyropes occurs under subsolidus conditions by the reaction of orthopyroxene and spinel in the presence of a fluid phase. The composition of the fluid was controlled by the interaction of water released by the decomposition of serpentine with carbonatite. The REEs released from the initial carbonatite were transported by the fluid and incorporated into the newly-formed garnet [35]. The presence of high-chromium lherzolitic pyropes with sinusoidal REE patterns provides evidence for the refertilization of the lithospheric mantle, i.e., harzburgite to lherzolite evolution, demonstrated by the near-vertical CaO–Cr<sub>2</sub>O<sub>3</sub> trend in pyrope compositions [15,29].

Low-chromium pyropes of lherzolitic and harzburgitic parageneses with sinusoidal REE patterns were numerous (19% of the total population) in the studied samples. To the best of our knowledge, this type of pyrope has not been reported in mantle peridotites from any kimberlite province. These pyropes (harzburgitic and lherzolitic) could have the same formation processes as the high-chromium pyropes with sinusoidal REE patterns, i.e., influenced by melts/fluids with high LREE/HREE ratios in an initial low-chromium harzburgitic source, followed by enrichment in CaO and refertilization of low-chromium lithospheric mantle. Additionally, these pyropes could have been formed by the reaction of melts/fluids having high LREE/HREE ratios with exsolved pyropes [15].

## 5.2. Evolution and Metasomatism of Lithospheric Mantle beneath the Southern Arkhangelsk Region

The following model of lithospheric mantle formation beneath the southern Arkhangelsk region is proposed. The model is graphically summarized in Figure 6.

In the first stage, the lithospheric mantle, composed of fertile peridotites, experienced different degrees of partial melting. Most likely, after low melting degrees (<35%), peridotites containing pyropes with fractionated MREE–HREE patterns formed. These peridotites constituted an ~50 km-thick layer at depths of ~90–150 km in the lithospheric mantle. The increase in melting degrees (>35–50%) resulted in the formation of garnet and clinopyroxene-free harzburgite.

After depletion, the lithospheric mantle was modified by several episodes of metasomatic enrichment. Early metasomatism could have been related to the reaction of C–H–O melts/fluids having high LREE/HREE ratios and probably carbonatite composition with depleted harzburgite, which led to the formation of high-chromium harzburgitic pyropes with sinusoidal REE patterns and was associated with the start of diamond formation [12,13]. This process occurred in the deep part (>150 km) of the lithospheric mantle, and peridotites with this type of garnet were most likely sampled from depths of ~150–180 km.

The next episode was the refertilization of the lithospheric mantle, demonstrated by the near-vertical CaO/Cr<sub>2</sub>O<sub>3</sub> evolution of high-chromium harzburgite to high-chromium lherzolite pyrope compositions. This process occurred in the deepest part of the lithospheric mantle within the interval of ~180–200 km and did not exclude continued diamond formation [13]. The high CaO and LREE contents in pyropes indicate that clinopyroxene formation was scarce at this stage.

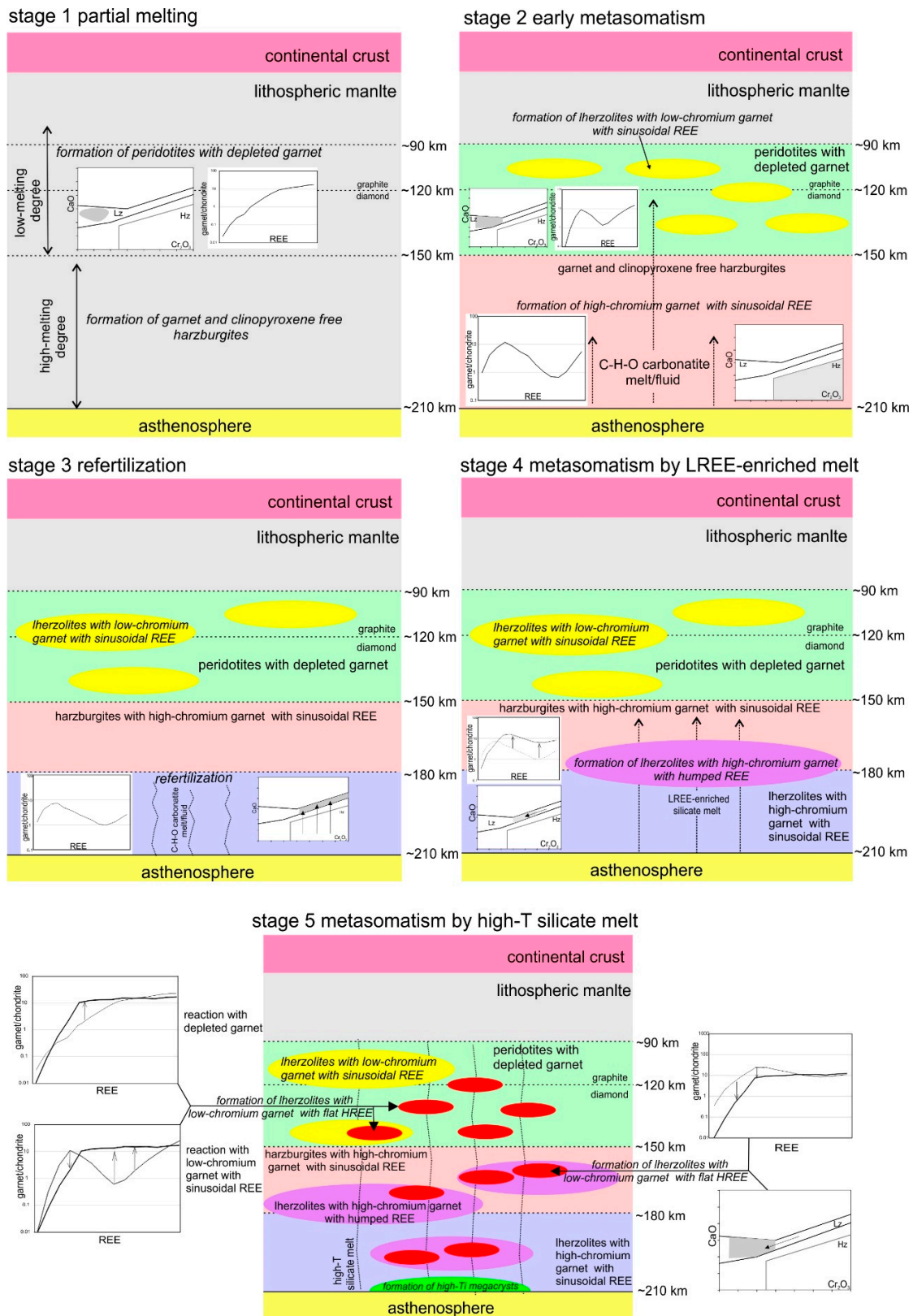


**Figure 6.** Schematic model of the evolution and metasomatism of lithospheric mantle beneath the southern Arkhanglesk region.

The next stage of metasomatic enrichment was related to the influence of high-temperature silicate melts with high LREE contents that led to the formation of pyropes with “humped” REE

patterns. These pyropes show concurrent decreases in CaO and Cr<sub>2</sub>O<sub>3</sub> and progressive overprinting by REEs. This type of metasomatism influenced the deep part of the lithospheric mantle at depths of ~150–200 km.

The final episode was characterized by the influence of high-temperature silicate melts, probably of basaltic composition, resulting in a concurrent decrease in CaO-Cr<sub>2</sub>O<sub>3</sub>, depletions in LREEs, and enrichments in Y in pyropes, which were equilibrated with clinopyroxene, i.e., the typical low-chromium lherzolitic paragenesis. Diamond formation could not have been associated with this stage because such metasomatic melts would effectively oxidize diamonds [36] and could totally destroy them [37]. This process occurred within a wide range of depths from ~90–200 km.

The pyropes of megacryst associations had the highest temperature estimates (>1300 °C), which provides evidence of their formation near the lithosphere-asthenosphere boundary, probably shortly before kimberlite eruption.

The formation of low-chromium pyropes with sinusoidal REE patterns in harzburgites and the subsequent evolution of pyrope composition from low-chromium harzburgite to lherzolites could have been associated with those of high-chromium varieties, i.e., similar to the early stage of metasomatism under the influence of C–H–O melts/fluids with high LREE/HREE ratios. However, the Ni thermometry placed these pyropes in the depth interval of ~90–150 km, mostly in the graphite stability field, which does not correlate with the depths of high-chromium pyropes (>150 km); this contradiction introduces some inconsistencies and ambiguities to the proposed model and casts doubt on the possibility of diamond crystallization or preservation at this stage. Additionally, low-chromium pyropes with sinusoidal REE patterns could be formed by the reaction of LREE-enriched melts with exsolved garnets [15].

In summary, the shallow part (<150 km) of the lithospheric mantle beneath the study area can be concluded to have been intensely metasomatized by high-temperature silicate melts, nevertheless preserving peridotites with residual pyropes at depths of 90–150 km. The lower part (150–200 km) of the lithospheric mantle was intensely affected by both silicate and carbonatite types of metasomatism, the latter being predominant.

### 5.3. Diamond Exploration Potential of the Southern Arkhangelsk Region

To assess the diamond exploration potential of any area of interest, solving two main problems is necessary. The first problem is revealing the suitability of the lithospheric mantle beneath the studied areas for the formation and preservation of diamonds. The second problem is the evaluation of the diamond content of kimberlites, which can be hosted within an area. The current results, obtained from Cr-pyrope geochemistry, allowed the solution of these problems.

The lithospheric mantle beneath the study area was composed of different types of mantle rocks, represented by dominant lherzolite and subordinate wehrlite, harzburgite-dunite, deformed lherzolite, and megacrysts, which are typical from the lithospheric mantle beneath kimberlite provinces worldwide. Cr-diopside thermobarometry delineated a mostly cold cratonic geotherm between 35 and 40 mW/m<sup>2</sup>, similar to the ADP lithospheric mantle, and the diamond stability field was encountered at temperatures of ~800–1000 °C with a thickness of ~100 km. The metasomatic enrichment of the lithospheric mantle was recorded by pyrope compositions similar to those beneath diamondiferous localities, e.g., the ADP and Siberian craton. The significant percentage (15%) of diamond-associated pyropes, i.e., the high-chromium pyropes of harzburgitic and lherzolitic parageneses with sinusoidal and “humped” REE patterns, emphasized the likelihood of high diamond contents in kimberlites to be discovered within the study area. A high proportion of garnets with fractionated MREE/HREE patterns was similar to the very diamondiferous Mir pipe (4–5 ct/t, [18]), which also favors the diamond prospects of the territory.

## 6. Conclusions

The interpretation of pyrope geochemistry provided the first information about the composition, structure, and metasomatic enrichment of the ~200 km-thick lithospheric mantle beneath the poorly-studied ancient Shenkursk craton within the northern East European platform. The lithospheric mantle has strong affinities with diamonds. These data suggest that the study area is worthy of further diamond exploration with a high probability of discovering new diamondiferous kimberlites. Current and previously-obtained [2] results confirmed the great diamond potential of the unexplored northeast European platform, particularly within the Arkhangelsk region territories.

**Supplementary Materials:** The following are available online at <http://www.mdpi.com/2075-163X/9/5/261/s1>: Table S1: Major (wt.%) and trace (ppm) element composition of garnet and estimated temperature (°C).

**Author Contributions:** Conceptualization, E.V.S.; methodology, E.V.S. and A.M.A.; resources, E.V.S., A.M.A., and V.S.S.; writing, original draft preparation, E.V.S.; funding acquisition, E.V.S.

**Funding:** This research was funded by the Russian Science Foundation Grant Number 17-77-10008 to Elena Shchukina. The fieldwork and sampling were done on state assignment of IGM SB RAS.

**Acknowledgments:** This manuscript has benefited from the helpful comments of two anonymous reviewers.

**Conflicts of Interest:** The authors declare no conflict of interest.

## References

1. Smit, K.V.; Shor, R. Geology and development of the Lomonosov diamond deposit, Northwestern Russia. *Gems Gemol.* **2017**, *53*, 144–167.
2. Shchukina, E.V.; Shchukin, V.S. Diamond Exploration Potential of the Northern East European Platform. *Minerals* **2018**, *8*, 189. [[CrossRef](#)]
3. Shchukin, V.S. Timan Aulacogen and Its Diamond Bearing Potential. Ph.D. Thesis, TSNIGRI, Moscow, Russia, 1986. (In Russian).
4. Koldaev, S.M. *Creation of Mineralogical and Geochemical Basis for the Area P-37-XXI, XXII, XXVII, XXVIII*; Territorial Regional Geological Fund; TSNIGRI: Moscow, Russia, 1991; p. 98. (In Russian)
5. Golubev, Yu.K. *Assessment of Diamond Content of the Ruch'evsky, Lachskaya, and Kargopol Areas for Further Exploration*; Territorial Regional Geological Fund; TSNIGRI: Moscow, Russia, 1993. (In Russian)
6. Lavrent'ev, Yu.G.; Korolyuk, V.N.; Usova, L.V.; Nigmatulina, E.N. Electron probe microanalysis of rock-forming minerals with a JXA-8100 electron probe microanalyzer. *Russ. Geol. Geophys.* **2015**, *56*, 1428–1436. [[CrossRef](#)]
7. Korolyuk, V.N.; Lavrent'ev, Yu.G.; Usova, L.V.; Nigmatulina, E.N. JXA-8100 microanalyzer: Accuracy of analysis of rock-forming minerals. *Russ. Geol. Geophys. (Geol. Geofiz.)* **2008**, *49*, 165–168. [[CrossRef](#)]
8. Horn, I.; Hinton, R.W.; Jackson, S.E.; Longerich, H.P. Ultra-trace element analysis of NIST SRM 616 and 614 using laser ablation microprobe-inductively coupled plasmamass spectrometry (LAM-ICP-MS): A comparison with secondary ion mass spectrometry (SIMS). *Geostand. Newslett.* **1997**, *21*, 191–203. [[CrossRef](#)]
9. Ryan, C.G.; Griffin, W.L.; Pearson, N.J. Garnet geotherms: Pressure-temperature data from Cr-pyrope garnet xenocrysts in volcanic rocks. *J. Geophys. Res.* **1996**, *101*, 5611–5625. [[CrossRef](#)]
10. Sobolev, N.V.; Lavrentyev, Y.G.; Pokhilenko, N.P.; Usova, L.V. Chrome-rich garnets from the kimberlites of Yakutia and their parageneses. *Contrib. Mineral. Petrol.* **1973**, *40*, 39–52. [[CrossRef](#)]
11. McDonough, W.F.; Sun, S.S. The composition of the Earth. *Chem. Geol.* **1995**, *120*, 223–253. [[CrossRef](#)]
12. Stachel, T.; Viljoen, K.S.; Brey, G.; Harris, J.W. Metasomatic processes in lherzolitic and harzburgitic domains of diamondiferous lithospheric mantle. *Earth Planet. Sci. Lett.* **1998**, *159*, 1–12. [[CrossRef](#)]
13. Stachel, T.; Aulbach, S.; Brey, G.P.; Harris, J.W.; Leost, I.; Tappert, R.; Viljoen, K.S. The trace element composition of silicate inclusions in diamonds: A review. *Lithos* **2004**, *77*, 1–19. [[CrossRef](#)]
14. Shchukina, E.V.; Agashev, A.M.; Kostrovitsky, S.I.; Pokhilenko, N.P. Metasomatic processes in the lithospheric mantle beneath the V. Grib kimberlite pipe (Arkhangelsk diamondiferous province). *Russ. Geol. Geophys.* **2015**, *56*, 1701–1716. [[CrossRef](#)]
15. Shchukina, E.V.; Agashev, A.M.; Pokhilenko, N.P. Metasomatic origin of garnet xenocrysts from the V. Grib kimberlite pipe, Arkhangelsk region, NW Russia. *Geosci. Front.* **2017**, *8*, 641–651. [[CrossRef](#)]

16. Kostrovitsky, S.I.; Malkovets, V.G.; Verichev, E.M.; Garanin, V.K.; Suvorova, L.V. Megacrysts from the V. Grib kimberlite pipe. *Lithos* **2004**, *77*, 511–523. [[CrossRef](#)]
17. Kopylova, M.G.; Nowell, G.M.; Pearson, D.G.; Markovic, G. Crystallization of megacrysts from protokimberlitic fluids: Geochemical evidence from high-Cr megacrysts in the Jericho kimberlite. *Lithos* **2009**, *112S*, 284–295. [[CrossRef](#)]
18. Agashev, A.M.; Serov, I.V.; Tolstov, A.V.; Shchukina, E.V.; Ragozin, A.L.; Pokhilenko, N.P. New genetic classification of lithospheric mantle garnets. In Proceedings of the 5th Russian Scientific and Practical Conference “Efficiency of geological exploration for diamonds: Prospects, resource, methodology and innovative-technological aspects”, Mirny, Russia, 29 May–1 June 2018; pp. 338–342. (In Russian).
19. Agashev, A.M.; Ionov, D.A.; Pokhilenko, N.P.; Golovin, A.V.; Cherepanova, Yu.; Sharygin, I.S. Metasomatism in the lithospheric mantle roots: Constraints from WR and minerals chemical composition of deformed peridotite xenoliths from the Udachnaya kimberlite pipe. *Lithos* **2013**, *160–161*, 201–215. [[CrossRef](#)]
20. Tappert, R.; Stachel, T.; Harris, J.W.; Muehlenbachs, K.; Ludwig, T.; Brey, G.P. Diamonds from Jagersfontein (South Africa): Messengers from the sublithospheric mantle. *Contrib. Mineral. Petr.* **2005**, *150*, 505–522. [[CrossRef](#)]
21. Griffin, W.L.; Shee, S.R.; Ryan, C.G.; Win, T.T.; Wyatt, B.A. Harzburgite to lherzolite and back again: Metasomatic processes in ultramafic xenoliths from the Wesselton kimberlite, Kimberly, South Africa. *Contrib. Mineral. Petrol.* **1999**, *134*, 232–250. [[CrossRef](#)]
22. Hasterok, D.; Chapman, D.S. Heat production and geotherms for the continental lithosphere. *Earth Planet. Sci. Lett.* **2011**, *307*, 59–70. [[CrossRef](#)]
23. Doucet, L.S.; Ionov, D.A.; Golovin, A.V. The origin of coarse garnet peridotites in cratonic lithosphere: New data on xenoliths from the Udachnaya kimberlite, central Siberia. *Contrib. Mineral. Petrol.* **2013**, *165*, 1225–1242. [[CrossRef](#)]
24. Dawson, J.B. A fertile harzburgite garnet lherzolite transition: possible inferences for the roles of strain and metasomatism in upper mantle peridotites. *Lithos* **2004**, *77*, 553–569. [[CrossRef](#)]
25. MacGregor, I.D. The reaction 4 Enstatite + Spinel = Forsterite + Pyrope. In *Carnegie Inst. Year Book 63*; Carnegie Inst.: Washington, DC, USA, 1964; p. 157.
26. Stachel, T.; Banas, A.; Aulbach, S.; Smit, K.V.; Wescott, P.; Chinn, I.L.; Julie Kong, J. The Victor Mine (Superior Craton, Canada): Neoproterozoic lherzolitic diamonds from a thermally-modified cratonic root. *Mineral. Petrol.* **2018**, *112*, S325–S326. [[CrossRef](#)]
27. Gregoire, M.; Bell, D.R.; Le Roex, A.P. Garnet lherzolites from the Kaapvaal craton (South Africa): Trace element evidence for a metasomatic history. *J. Petrol.* **2003**, *44*, 629–657. [[CrossRef](#)]
28. Stachel, T.; Harris, J.W. The origin of cratonic diamonds—Constraints from mineral inclusions. *Ore Geol. Rev.* **2008**, *34*, 5–32. [[CrossRef](#)]
29. Howarth, G.H.; Barry, P.H.; Pernet-Fisher, J.F.; Baziotis, I.P.; Pokhilenko, N.P.; Pokhilenko, L.N.; Bodnar, R.J.; Taylor, L.A.; Agashev, A.M. Superplume metasomatism: Evidence from Siberian mantle xenoliths. *Lithos* **2014**, *184–187*, 209–224. [[CrossRef](#)]
30. Moore, A.; Belousova, E. Crystallization of Cr-poor and Cr-rich megacryst suites from the host kimberlite magma: Implications for mantle structure and the generation of kimberlite magmas. *Contrib. Mineral. Petrol.* **2005**, *149*, 462–481. [[CrossRef](#)]
31. Jones, R.A. Strontium and Neodymium isotope and rare earth element evidence for the genesis of megacrysts in kimberlites of southern Africa. In *Mantle Xenoliths*; Nixon, P.H., Ed.; Wiley: New York, NY, USA, 1987; pp. 711–724.
32. Davies, G.R.; Spriggs, A.J.; Nixon, P.H. A non-cognate origin for the Gibeon kimberlite megacryst suite, Namibia: Implications for the origin of Namibian kimberlites. *J. Petrol.* **2001**, *42*, 159–172. [[CrossRef](#)]
33. Nimis, P.; Zanetti, A.; Dencker, I.; Sobolev, N.V. Major and trace element composition of chromian diopsides from the Zagadochnaya kimberlite (Yakutia, Russia): Metasomatic processes, thermobarometry and diamond potential. *Lithos* **2009**, *112*, 397–412. [[CrossRef](#)]
34. Shu, Q.; Brey, G.P. Ancient mantle metasomatism recorded in subcalcic garnet xenocrysts: Temporal links between mantle metasomatism, diamond growth and crustal tectonomagmatism. *Earth Planet. Sci. Lett.* **2015**, *418*, 27–39. [[CrossRef](#)]

35. Chepurov, A.A.; Faryad, S.W.; Agashev, A.M.; Strnad, L.; Jedlicka, R.; Turkin, A.I.; Mihaljevic, M.; Lin, V.V. Experimental crystallization of a subcalcic Cr-rich pyrope in the presence of REE-bearing carbonatite. *Chem. Geol.* **2019**, *509*, 103–114. [[CrossRef](#)]
36. Rorbach, A.; Schmidt, M.W. Redox freezing and melting in the Earth's deep mantle resulting from carbon–iron redox coupling. *Nature* **2011**, *472*, 209–212. [[CrossRef](#)]
37. Bataleva, Y.V.; Palyanov, Y.N.; Sokol, A.G.; Borzdov, Y.M.; Palyanova, G.A. Conditions for the origin of oxidized carbonate–silicate melts: Implications for mantle metasomatism and diamond formation. *Lithos* **2012**, *128–131*, 113–125. [[CrossRef](#)]



© 2019 by the authors. Licensee MDPI, Basel, Switzerland. This article is an open access article distributed under the terms and conditions of the Creative Commons Attribution (CC BY) license (<http://creativecommons.org/licenses/by/4.0/>).